P-ISSN 2586-9000
E-ISSN 2586-9027
Homepage : https://tci-thaijo.org/index.php/SciTechAsia
Science & Technology Asia
Vol. 26 No.3 July - September 2021
Page: [64-76]
Original research article

Development of Vehicle Chassis from Novel Materials for Light Weight Electric Shuttles Using Finite Element Analysis

Snunkhaem Echaroj, Nattadon Pannucharoenwong*, Phadungsak Rattanadecho

Department of Mechanical Engineering, Faculty of Engineering, Thammasat University, Pathum Thani 12120, Thailand

Received 21 February 2020; Received in revised form 7 July 2020
Accepted 14 September 2020; Available online 6 September 2021

ABSTRACT

This research aimed to evaluate the impact of the z-axis forces on stress and total deformation for the chassis of a 23 passenger electric shuttle bus. Track testing protocols were also developed and performed on the electric shuttle bus to investigate the effectiveness of battery and comfort based on noise and vibration for a total distance of 1,000 km. Simulation was validated by measuring stress and deformation using an attachable strain gauge and a dial indicator. Five different types of materials were used to simulate the chassis including steel, high carbon steel, AMS4122 aluminum alloy, AMS4119 aluminum alloy and AZ31B magnesium alloy. Simulation results showed maximum deformation of 2.22 mm for AZ31B magnesium alloy, 1.42 mm for AMS4119 aluminum alloy, 1.01 mm for steel, 0.47 mm for AMS4122 aluminum alloy, and 0.16 mm for high carbon steel. On the other hand, aluminum and magnesium alloy weighted almost 50% less than steel and high carbon steel. It can be concluded that AMS4122 aluminum alloy is the most suitable material for chassis construction due to its light weight and lowest total deformation of the chassis structure.

Keywords: Aluminum alloy; Chassis; Elective shuttle bus; Finite element; Magnesium alloy

1. Introduction

Due to the petroleum shortage crisis, automotive industries around the world have turned their attention to electric vehicles, which rely only on electricity and high energy density batteries such as the Lithium-ion battery. Petroleum oil consumption in the transportation sector was as high as 63% in 2015, which was a significant increase from 43% in 1975 [1]. Meanwhile, transport activities caused almost 20% of total Green House Gas emission in Europe [2]. Additionally, an increase in the local transportation and logistics requirements has accelerated the development of robust electric shuttles. For these reasons, the demand for EV shuttle buses is estimated to grow approximately 17% by year 2030 [3].

***Corresponding author:** pnattado@engr.tu.ac.th

A logistic system is also an essential part of a smart city plan developed in different countries. The Ministry of Energy in Thailand proposed a 3 phase plan for establishing a sustainable smart city, which requires the production of approximately 1.2 million EV passengers by year 2036 [4]. In order to fulfill this requirement it is important to develop the most effective blueprint and manufacturing details for an EV shuttle bus. It is also important to reduce the weight of the chassis in order to compensate for the increase in weight due to the presence of the batteries.

Among the various automobile components, chassis structure is one of the most important parts. An outstanding chassis is defined as a structure capable of absorbing immediate bending load, torsional load and shock load while minimizing the deformation or damage of the adjacent components, and maximizing passenger comfort and driver handling. Chassis performance in terms of automobile handling can be improved by weight reduction. Additionally, long-term exposure to uniaxial dynamic load can result in material fatigue failure. The finite element method (FEM) is employed to minimize deformation of chassis structure and simulate the stress profile along the materials. For instance, Radford reported the simulated effect of the addition of cockpit stiffener on motorsports automobile chassis deformation [5]. Critical stress point in the heavy duty truck chassis can be located using the software-assisted FEM to evaluate potential long-term fatigue problems [6]. Karahna et al. reported the optimum thickness of a steel-based truck chassis by using software-assisted FEM [7]. In order to benefit most from the software-assisted FEM it is important to study material theoretical properties. Hanisha et al. development finite element analysis for simulation of cold formed steel used to construct beam-column joints [8]. Another research simulated pyroelectric materials used for energy harvesting and medicine by employing finite element analysis [9].

Basic engineering applications dictate that metal materials exist in a 3-dimensional stress state where deformation characteristic of metals under either triaxial unloading or loading corresponds with the real environment. Investigation of the beginning and propagation behavior of macroscopic cracks and deformation lead to accurate development of preventive protocol for automotive structural engineering. There are three different types of material deformation including twining, slip and dislocation deformation. Simulation of material deformation and stress are based on the numerical derivation of thermal gradient according to Fourier's Law [10].

The degree of deformation of metal is directly proportional to the magnitude of stacking faults created during particle growth [11]. Taheri et al. reported the application of elasticity modulus and Poisson's ratio for calculating damage build-up of the material [12]. Prediction of material lifetime can be accomplished by inputting time and temperature in the Larson-Miller parameter which is based on the Arrhenius rate equation [13]. Temperature of the environment during deformation was also found to have a significant effect on dislocation and boundary mobility [14-15]. However, ultimate stress of the nanocrystalline palladium can be enhanced by increasing the relaxation stress time [16-17].

A finite element method (FEM) can be used to simulate and optimize material structure. Application of FEM to simulate stress and deformation potential can significantly lower the cost of the experiment. Applications of FEM include investigation of the effect of welding sequence on the nonlinear elastoplasticity of 6061-T6 aluminum alloy used as automobile components [18-19], automobile crashing simulation [20-21] and automobile chassis development [22-24]. To the best of the researchers' knowledge very little insight has

been shed on the effect of material type and thickness on the stress and deformation profile of an EV shuttle bus chassis. A new chassis design has been proposed to improve stability and lower stress accumulation. One of the main challenges in development of an electric vehicle is in the weight of the chassis. Weight reduction is the main concern in the automotive industry. Many different types of materials have been proposed, including aluminum alloy and magnesium alloy, as components in aeroplane [25]. However, to the best of our knowledge, no research has studied their potential.

The purpose of this paper is to offer an overview of the application of a software-assisted FEM approach in the fundamental understanding and parametric investigation of an automobile chassis. Track performance testing was conducted for 1000 km in order to prepare the chassis for stress and deformation testing and also to measure the electric motor temperature. Simulation of stress and deformation was performed on the chassis of a 23 passenger electric shuttle bus. Mechanical properties of steel were tested and data was input into the simulation software. Different types of materials were used in the finite element analysis, including steel, high carbon steel, two aluminum alloys and magnesium alloy. Comparisons of different material types under the same load were reported.

2. Experimental Setup

2.1 Governing equation

The governing equation used for simulating stress and deformation of a dynamic structure is usually in the form of partial differential equation (PDE). The general algorithm employed in most cases is shown in Eq. (2.1).

$$n\frac{\partial^2 y}{\partial t^2}u + w\frac{\partial y}{\partial t} + \nabla\cdot(-c\nabla y - \alpha y + \gamma) + \beta\cdot\nabla y + by - g = 0, \quad (2.1)$$

where the PDE consisted of real coordinate space of n dimensions, y represents the dependent variable that needs to be calculated, coefficients $(\mathrm{n}, \mathrm{w}, \mathrm{b}, \mathrm{g})$ are scalar, and coefficients (α, β, γ) are vectors.

For a static structure in equilibrium the partial equation for stress is reduced to equation of equilibrium in the three coordinate system as shown in Eqs. (2.2)-(2.4) (x direction, y-direction and z-direction).

$$\frac{\partial \sigma_{xx}}{\partial x} + \frac{\partial \sigma_{xy}}{\partial y} + \frac{\partial \sigma_{xz}}{\partial z} + b_x = 0, \quad (2.2)$$

$$\frac{\partial \sigma_{yx}}{\partial x} + \frac{\partial \sigma_{yy}}{\partial y} + \frac{\partial \sigma_{yz}}{\partial z} + b_y = 0, \quad (2.3)$$

$$\frac{\partial \sigma_{zx}}{\partial x} + \frac{\partial \sigma_{zy}}{\partial y} + \frac{\partial \sigma_{zz}}{\partial z} + b_z = 0. \quad (2.4)$$

Material deformation is calculated by applying the strain-displacement relations. The displacement gradient of the three coordinate system, as shown in Eqs. (2.5)-(2.6), indicates the rate of change in the displacement of a particular point in the material.

$$\varepsilon_{xx} = \frac{\partial u_x}{\partial x}, \varepsilon_{yy} = \frac{\partial u_y}{\partial y}, \varepsilon_{zz} = \frac{\partial u_z}{\partial z}, \quad (2.5)$$

$$\varepsilon_{xy} = \frac{1}{2}\left(\frac{\partial u_x}{\partial y} + \frac{\partial u_y}{\partial x}\right), \varepsilon_{xz} = \frac{1}{2}\left(\frac{\partial u_x}{\partial z} + \frac{\partial u_z}{\partial x}\right),$$

$$\varepsilon_{yz} = \frac{1}{2}\left(\frac{\partial u_y}{\partial z} + \frac{\partial u_z}{\partial y}\right). \quad (2.6)$$

A superposition technique was employed to combine and generalize the stress components from various loads. The resulting equations are referred to as generalized Hooke's Law. In order for this method to be accurate, stress produced must be linearly proportional to the load and the given model deforms slightly compared with the whole structure. Therefore, the multiaxial loading of a homogeneous isotropic material can be expressed through Eqs. (2.7)-(2.9).

$$\varepsilon_x = \frac{1}{E}\left(\sigma_x - v\sigma_y - v\sigma_z\right), \quad (2.7)$$

$$\varepsilon_y = \frac{1}{E}\left(-v\sigma_x + \sigma_y - v\sigma_z\right), \quad (2.8)$$

$$\varepsilon_z = \frac{1}{E}\left(-v\sigma_x - v\sigma_y + \sigma_z\right). \quad (2.9)$$

The above Eqs. (2.2)-(2.8) are dedicated to the calculation of direct bending stress and deformation. However, in addition to direct and bending stress, real application of EV shuttle will also incorporate torsional force due to uneven roads. For this reason, it is important to combine both bending and torsional force that act on the chassis of the EV shuttle during movement. Eqs. (2.10) and (2.11) represent torsional stress and deformation of a simple rectangular object which represent metal beams that are connected to create the chassis.

$$\sigma_{com} = \frac{\sigma_d + \sigma_b}{2} \pm \sqrt{\left(\frac{\sigma_d - \sigma_b}{2}\right)^2 - \tau^2}, \quad (2.10)$$

where σ_d represents direct stress, σ_b represents bending stress and τ represents torsional stress.

Uneven road surface structure will cause the chassis to experience vibration at a specific frequency. This is also an important criteria for assessing the dynamic behavior of the chassis. Eq. (2.11) expresses natural frequency of an object as a function of mass of the object and stiffness value.

$$\omega_f = \frac{1}{2\pi}\sqrt{\frac{k_{eq}}{M}}. \quad (2.11)$$

2.2 Electric shuttle bus specification and track performance-testing protocols

An image of the electric shuttle bus is shown in Fig. 1. The specifications of the EV shuttle bus are shown in Table 1. Generally, the EV shuttle bus can carry 23 people and consists of a 9 kW electric motor connected to 24 boxes of 6V (225 amps) batteries. The suspension contains leaf springs and a hydraulic shock absorber. The body frame is made of fiber glass and the chassis is made from black steel. The maximum speed allowed by the controller is 35 km/h and it was declared that the EV shuttle can cover 120 km after each full charge.

Fig. 1. EV shuttle bus used for the testing and simulation.

Table 1. EV shuttle bus specification.

Specification	Value
Passenger seats (person; 60 kg per person)	23
Material type	Steel
Battery	6V 225 amps (24 boxes)
Electric motor	45V, 9kW
Suspension	Leaf spring – hydraulic shock absorber
Maximum speed	35 km/h
Longest distance	120 km
Elevated slope	15%
Brake distance	6 m
Shuttle bus dimension (width, length, height) mm.	1,820 x 5,500 x 2,160
Turning radius	<8.5 m
Maximum weight	1,750 kg

After obtaining the 23 passenger electric shuttle, the vehicle was tested to evaluate driving performance under protocols as shown in Table 2. The protocols consist of 4 major condition variations including vehicle speed (normal economic = 20 km/h, aggressive = >25 km/h), weight of dummies added, accessories status and solar status. Accessories included front light, rear light, radio and internal light. For the "Accessories on" protocol all lights were turned on, including the radio inside the shuttle bus, to simulate full-scale energy consumption during performance testing. A solar roof-top was installed at the top of the shuttle bus. For "Solar On" protocol the driver will turn on the solar cell during performance testing. The test track is concrete with different elevations of terrain including flat, 5° slope and 7° slope. Each track cycle covered approximately 2.6 km. The total distance covered during the entire track testing is 1000 km. The testing conditions for the 12 days tracking testing are shown in Table 1. In addition to the analysis of chassis structure deformation and battery conditions, the track testing protocols were also developed to evaluate the comfort of the vehicle, which includes both vibrational and acoustic comfort. These two conditions are linked to noises that occur after long-term usage of vehicles.

Table 2. Test track protocols for 1,000 km performance testing.

Day	Speed (km/h)	Weight added (kg)	Driving behavior	Accessories status	Solar status
1	20	0	Normal economic	Off	Off
2	20	1300	Normal economic	Off	Off
3	>25	0	Aggressive	Off	Off
4	>25	1300	Aggressive	On	Off
5	20	0	Normal economic	Off	Off
6	20	1300	Normal economic	Off	Off
7	>25	0	Aggressive	Off	Off
8	>25	1300	Aggressive	On	Off
9	20	0	Normal economic	Off	On
10	20	1300	Normal economic	Off	On
11	>25	0	Aggressive	Off	On
12	20	1300	Aggressive	On	On

2.3 Simulation conditions, chassis material and validation

ANSYS software was employed to construct a three-dimensional numerical model that accurately generates stress and deformation of the chassis subject to simulated load and constraints. The chassis geometry used for finite element analysis was formed in NX Siemen software. After the geometry was exported to ANSYS software, it was important to merge all components of the chassis in order to avoid problems regarding the degree of freedom and emergence of non-convergence conditions.

The load considered in the simulation increased the weight of batteries (28 kg each), electric motor/controller set (126 kg), passengers (assumed 60 kg per person) and EV fiberglass body as shown in Fig.2. The weight of the fiberglass body was equally distributed along the chassis. Fixed point constraints were located on the wheels of the chassis. The chassis was made of steel and weighed approximately 1,100 kg. Steel used to construct the chassis was assumed to be isotropic and a homogeneous material. Mechanical properties of the isotropic chassis steel were found using tensile testing (Instron 5969) and hardness testing apparatus, as shown in Table 3.

In addition to steel, other types of material were simulated including high carbon steel, AMS4119 (aluminum alloy, AMS4122 (aluminum alloy), and AZ31B (magnesium alloy). Mechanical properties

of high carbon steel and alloy materials were found in the literature [26-27]. The mechanical properties and metal composition of these materials are shown in Table 3.

Validation of deformation length was performed using sand bags as a dummy load and a dial indicator (Mitutoyo 543-782 Lever Dial Indicator) to measure how much material deformed. Specific stresses were measured at different locations on the chassis using multiple resistance-type strain gauges (Showa N31 triaxial strain gage). The strain gauges were attached to the chassis using SHOWA 4000 Strain Gage Cyanoacrylate adhesive.

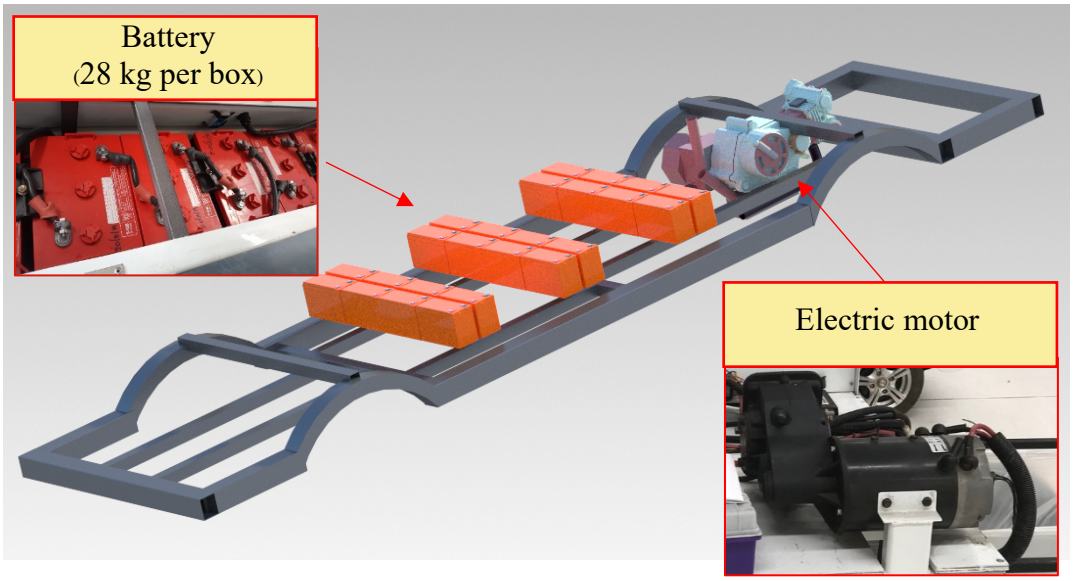

Fig. 2. Three-dimensional modeling of chassis, batteries and electric motor using CAD software.

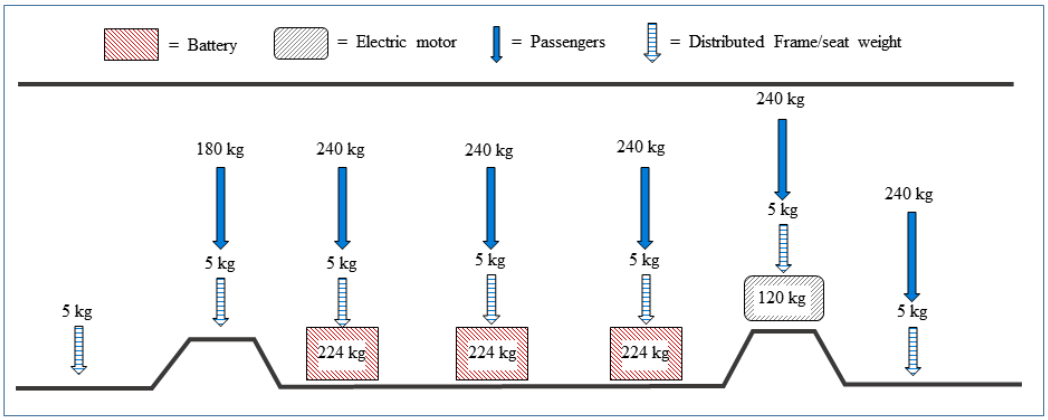

Fig. 3. Weight distribution of passengers, frame, electric motor and batteries on the chassis.

Table 3. Mechanical properties of material used to construct the chassis.

Mechanical properties	**Steel chassis (EV shuttle bus)**	**High Carbon Steel AISI 1065**	**AMS4122 (SAE 7075 T6)**	**AMS4119 (SAE 2024 T4)**	**AZ31B Magnesium alloy**
Tensile strength (MPa)	310 - 360	635	572	469	260
Yield strength (MPa)	180 - 240	490	503	324	200
Density (g/cm^3)	7.872	7.85	2.80	2.81	1.77
Composition (%)	Fe (99.18-99.62) C (0.080-0.13)	Fe (98.31 - 98.8) C (0.60 - 0.70)	Al (>90) Mg (2.1 – 2.9) Cr (0.18 – 0.40) Zn (5.1 – 6.1) Ti (0.2) Cu (1.2 – 2.0)	Al (>90) Mg (1.2-1.8) Cr (0.10) Zn (0.25) Cu (3.8 – 4.9)	Mg (97) Al (2.50 - 3.50) Zn (0.60 - 1.40) Cu (0.05)
Elastic modulus (GPa)	200	200	72	70 - 80	44.8
Poisson's ratio	0.27-0.30	0.27-0.30	0.33	0.33	0.35
Shear Modulus (GPa)	80.0	80	26.9	28.2	17
Shear Strength (MPa)	-	-	300	285	130
Elongation at break (%)	20	10	11	20	15
Hardness, Brinell 500 kg load, 10 mm ball	105	187	150	120	49

3. Results and Discussion

3.1 Track performance testing

The EV shuttle bus was tested for a total distance of 1,000 km (12 days). After day 4, a high pitch noise was detected in front and rear of the EV shuttle bus. Comfort performance was also evaluated based on noises generated from the vehicle [28]. A rattling noise was also observed to be generated from the roof. These noises indicated possible deformation of the chasis due to long duration of heavy load bearing. Inspection of the EV shuttle bus after 6 days of testing revealed a small crack in the fiberglass frame located in the front seat of the vehicle. This defect is associated with the imbalance vibration caused by a non-uniform load. The temperature of the electric motor after a complete track circuit was measured using an infrared temperature sensor. The temperature measured was in the range of 60 to 80°C depending on the load as shown in Figure 4a. On a very hot day and with a full load, the temperature reached as high as 79°C which caused the electric motor to automatically shut down.

3.2 Simulation validation

Simulated results of material stress and deformation were derived from software-based finite element analysis. These simulated results were compared with measured data obtained from the electric shuttle's chassis. Stress and deformation were measured at different locations, including 10 high stress points and 20 distinctive deformation points. The correlation between simulated and measured data was plotted in Fig. 4. Fig. 4 shows that simulation of the steel chassis to find stress and deformation is very close to measured data. Coefficient of determination (R^2) between the simulated and measured stress and deformation were 0.9282 and 0.9723, respectively.

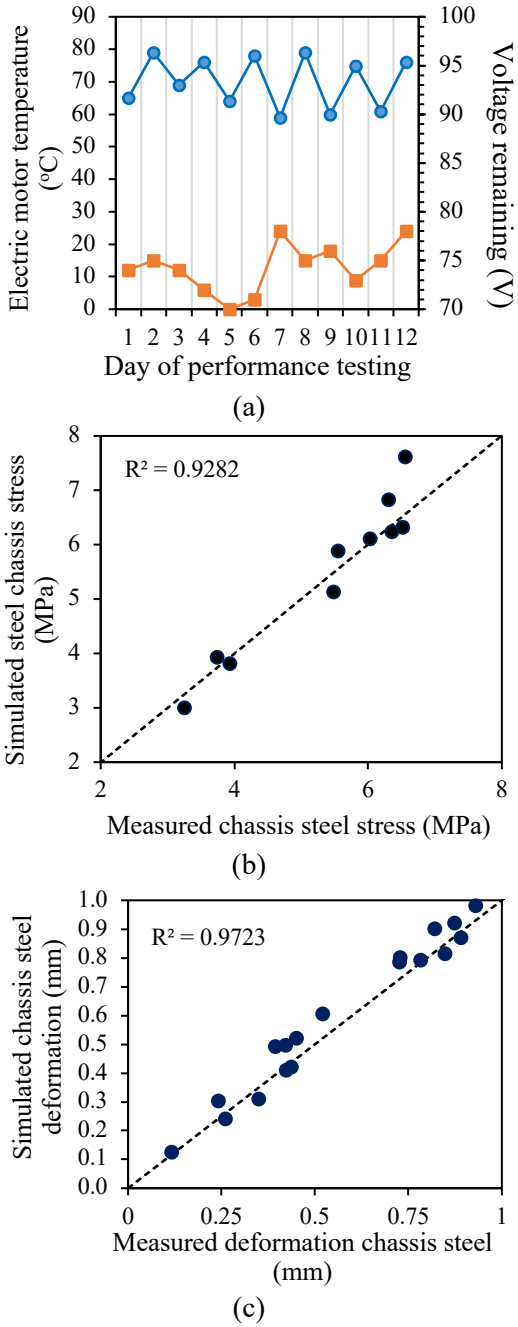

Fig. 4. Validation of simulated stress and total deformation of steel chasis with measured data.

3.3 Stress and deformation simulations

Figs. 5a and 5b show the simulation results of stress (MPa) and deformation (mm) for a chassis that is made out of AMS4122. Simulation of other types of materials (such as steel, high carbon steel,

and aluminium alloys) were also conducted but not shown in this manuscript because their simulated contours were similar to steel but with significantly different maxium stress and total deformation. The chassis made of magnesium alloy was found to bear a maximum stress of 23.492 MPa. High stress points are located in many joints, especially in areas of high force impact which were in the middle section of the chassis. These high stress points (depicted in light blue color) represent stress in the range of 5.5 to 7.4 MPa. Maximum deformation of approximately 2.22 mm was simulated for the magnesium alloy-based chassis, shown as the red area in Fig. 5b. The high deformation point of the chassis is located in the center of the chassis. This is because this part of the chassis is the farthest away from the fixed points (four contraints). In the simulation, forces from load acting on the chassis were assumed to be uniform. For this reason, the simulated deformation as shown in the figure below are symmetric in the y-axis.

The locations of high stress and deformation of other models for different materials are similiar to that of magnesium alloy. However, these models result in different maximum stresses and total deformations. A comparison between stress and total deformation simulated for each material is shown in Fig. 6. The largest deformation was observed for magnesium alloy (113% larger maximum total deformation compared with steel) and AMS4119 aluminum alloy (36% larger maximum total deformation compared with steel) in comparison with steel and high carbon steel. This simulated result corresponded well with simulation of a motorcycle chassis [29]. However, according to the inset in Fig. 6, a weight reduction of 40% was possible when magnesium and aluminum alloy were used instead of steel or high carbon steel. It is interesting to observed that even though AMS4122 is an aluminum alloy similar to AMS4119, it demonstrated a very stiff structure with maxiumum total deformation 55% lower than steel metal. This is due to the larger content of Zn metal in the AMS4122 type aluminium alloy. Therefore, according to this simulation, AMS4122 aluminum alloy is the most promising type of material that can reduce the weight of the chassis while maintaining a low deformation value compared with other type of material. Fig. 7 shows the maximum stress simulated for different type of materials. It was observed that HC bear the highest stress compared with other material.

One of the main challenges that manufacturers will need to overcome in order to effectively use AMS4122 type aluminium alloy to build a chassis is the connectivity between each metal piece. This is because aluminium alloy consists of various metals which will flow differently when exposed to high heat during welding. This can result in deformation and, potentially, cracks in the chassis structure after welding. Welding is very difficult for aluminium metal. To solve this problem a group of research has introduced a new nanoparticle into the structure during welding [30]. Since a shuttle bus contains only a chassis and an open body the simulation results would be quite different from a four-wheel closed EV.

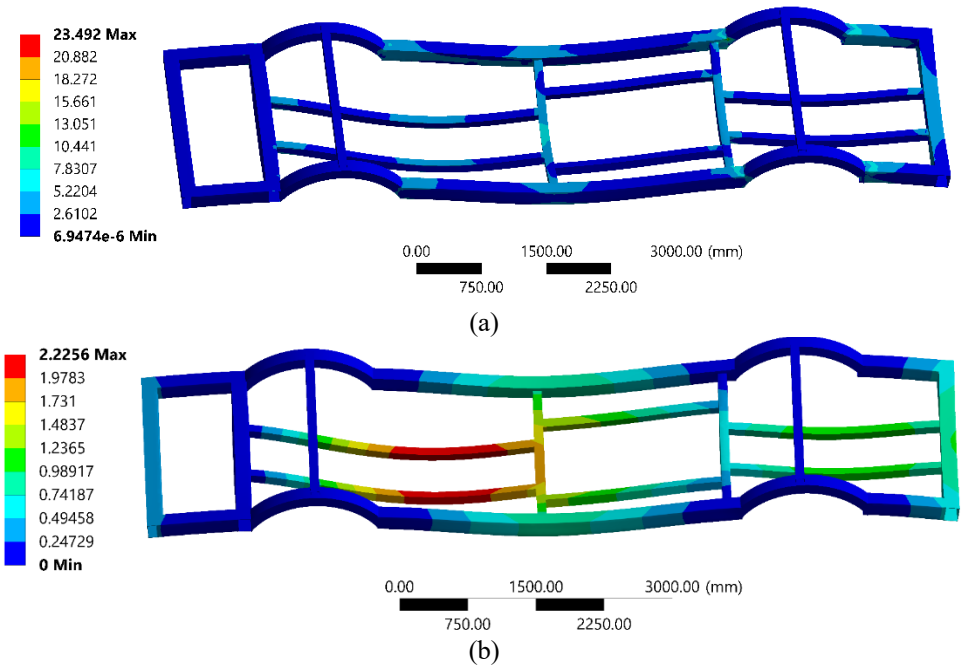

Fig. 5. Finite element simulation resutls of AMS4122 chassis illustrating material a) stress (MPa) and b) deformation (mm) from weight loads.

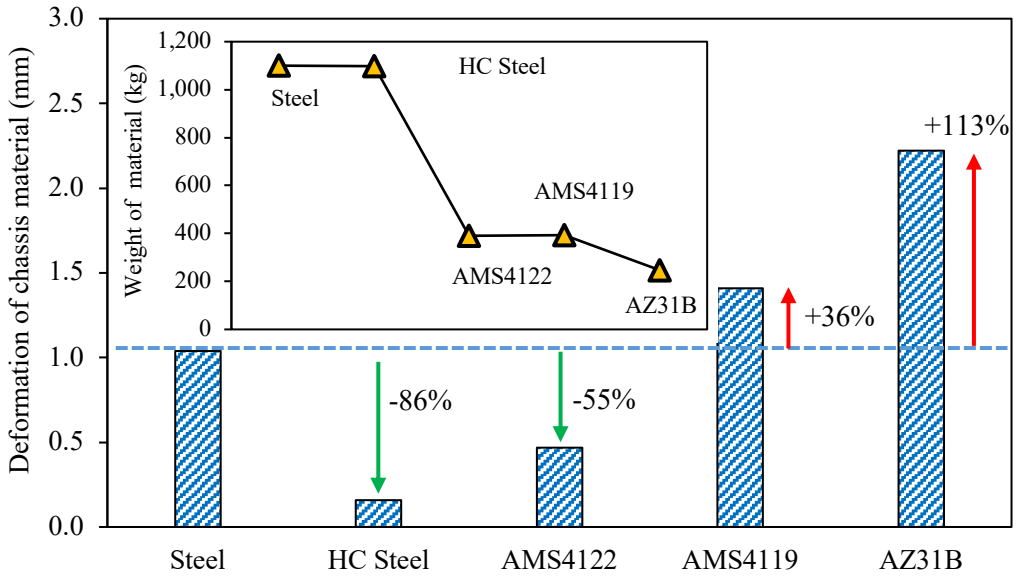

Fig. 6. Deformation comparison between different material type for chassis (inset: weight of the chassis made from different material).

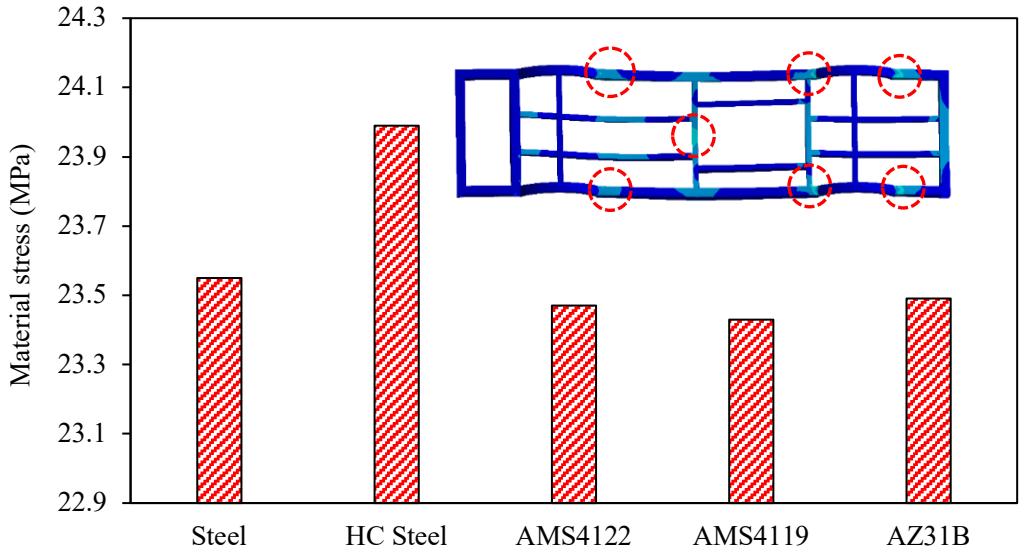

Fig. 7. Comparisons between stress of different materials for chassis (inset: top view image of chassis with high stress area located by a dash line circle.

4. Conclusion

Track testing of the electric shuttle bus revealed that the vehicle batteries could store enough electricity for a 120 km continuous drive per one complete charge cycle. The temperature measured at the electric motor averaged about 75 ºC. If the electric motor temperature exceeded 90 ºC the motor was found to shutdown immediately. Additionally, this study has demonstrated for the first time the benefit of using aluminum alloy as a material for construction of an electric shuttle bus chassis. Specifically, according to FE simulation, AMS4122 aluminum alloy was found to offer the lower maximum total deformation (0.47 mm) compared with conventional steel (1.02 mm). Both the aluminum and the magnesium alloy chassis also benefited from weight reduction in comparison with steel and high carbon steel. Simulation results for the steel chassis was found to correlate well with measured data with R^2 equal to 0.9282 and 0.9723 for stress and total deformation measurements. It would be interesting to construct a chassis from either aluminium or magnesium alloy to validate simulation data for alloy materials.

Acknowledgments

The authors gratefully acknowledge the support of the Program Management Unit for Human Resources & Institutional Development, Research and Innovation, NXPO (grant number B05F630092) and Thailand Science Research and Innovation Fundamental Fund (Project No. :66082) and Thammasat School of Engineering, Thammasat University for providing financial support for this work. This research appreciates the support of Bangpu Infinergy Co.Ltd.

References

[1] Key world energy statistics. International Energy Agency. 2016;1(1):1-88.

[2] Coussy P. Greenhouse gas emissions in the road transport sector: moving towards inclusion in the European system of CO2 allowances? IFP Energies nouvelles-Lyon. 2015.

[3] Greenwood M. Demand for Electric Buses and Trucks Is Expected to Soar. 2019; https://www.engineering.com/AdvancedManufacturing/ArticleID/18453/Demand-for-Electric-Buses-and-Trucks-Is-Expected-to-Soar.aspx.

[4] Thailand's Energy 4.0. Energy Policy and Planning Office; 2019.

[5] Radford DW. 3.14 Development of Composite Chassis for Motorsports. In: Beaumont PWR, Zweben CH, eds. Comprehensive Composite Materials II. Oxford: Elsevier; 2018:350-419.

[6] Kurdi O, Abdul Rahman R. Finite Element Analysis of Road Roughness Effect on Stress Distribution of Heavy Duty Truck Chassis. International Journal of Technology. 2010;1:57-64.

[7] Kahraman Y, Yılmazçoban İK. Truck chassis structural thickness optimization with the help of finite element technique. TOJSAT The Online Journal Of Science And Technology. 2011;1(3).

[8] Sri Sai Hanisha C, Siva Kishore I. Experimental and finite element analysis of cold formed steel beam-column joint. Materials Today: Proceedings. 2020.

[9] Magouh N, Dietze M, Bakhti H, Solterbeck C-H, Azrar L, Es-Souni M. Finite element analysis and EMA predictions of the dielectric and pyroelectric properties of 0-3 Pz59/PVDF-TrFE composites with experimental validation. Sensors and Actuators A: Physical. 2020;310:112073.

[10] Lee SH, Kim ES, Park JY, Choi J. Numerical analysis of thermal deformation and residual stress in automotive muffler by MIG welding. Journal of Computational Design and Engineering. 2018;5(4):382-90.

[11] Kim H-K, Kim S-H, Ahn J-P, Lee J-C. Deformation criterion for face-centered-cubic metal nanowires. Materials Science and Engineering: A. 2018;736:431-7.

[12] Peng K, Zhou J, Zou Q, Zhang J, Wu F. Effects of stress lower limit during cyclic loading and unloading on deformation characteristics of sandstones. Construction and Building Materials. 2019;217:202-15.

[13] Ou M, Ma Y, Xing W, et al. Stress rupture properties and deformation mechanisms of K4750 alloy at the range of 650 °C to 800 °C. Journal of Materials Science & Technology. 2019;35(7):1270-7.

[14] Detrois M, Antonov S, Tin S, Jablonski PD, Hawk JA. Hot deformation behavior and flow stress modeling of a Ni-based superalloy. Materials Characterization. 2019:109915.

[15] Pannucharoenwong, N., Rattanadecho, P., Timchenko, V., Echaroj, S., Nabudda, K. Investigation of double slope solar distillation efficiency using heat absorber made from zinc.Science and Technology Asia. 2019; 24(4): 70-82.

[16] Bachurin DV. Influence of internal stresses on deformation behavior of nanocrystalline palladium. Materials Science and Engineering: A. 2018;734:255-9.

[17] Pannucharoenwong, N., Rattanadecho, P., Echaroj, S., Hemathulin, S., Nabudda, K. The investigation of heat absorber on the efficiency of slanted double-slope solar distillation unit. International Journal of Heat and Technology. 2020;38(1): 171-9.

[18] Yi J, Zhang J-m, Cao S-f, Guo P-c. Effect of welding sequence on residual stress and deformation of 6061-T6 aluminium alloy automobile component. Transactions of Nonferrous Metals Society of China. 2019;29(2):287-95.

[19] Echaroj, S., Pannucharoenwong, N., Vengsungnle, P., Wichangarm, M. Effect of Geometric Design on Airflow Simulation Inside the Storage Room for Paddy.IOP Conference Series: Materials Science and Engineering. 2019;501(1):012040.

[20] Hickey A, Xiao S. Finite Element Modeling and Simulation of Car Crash. International Journal of Modern Studies in Mechanical Engineering. 2017;3(1).

[21] Jongpluempiti, J., Vengsungnle, P., Pannucharoenwong, N. Investigation of parameters affecting cotton waste shredding for as straw mushroom substrates. Asia-Pacific Journal of Science and Technology. 2019;24(1): 1-8.

[22] Santa Rao K, Musalaiah G, Chowdary K. Finite Element Analysis of a Four Wheeler Automobile Car Chassis. Indian Journal of Science and Technology. 2016;9.

[23] Gomonwattanapanich, O., Pannucharoenwong, N., Rattanadecho, P., Echaroj, S., Hemathulin, S. Vibration control of vehicle by active suspension with LQG algorithm.International Journal of Automotive and Mechanical Engineering. 2020; 17(2):8011-8.

[24] Gomonwattanapanich, O., Pannucharoenwong, N., Rattanadecho, P., Echaroj, S., Polprasert, J. Evaluation of the modified tustin friction compensation in simulation of the PID controller system for rotating-shaft dynamic. GMSARN International Journal. 2020;14(2): 54-8.

[25] Kaushik. A Review on use of Aluminium Alloys in Aircraft Components. i-manager's Journal on Material Science. 2015;3:33-8.

[26] Pervaiz M, Panthapulakkal S, Kc B, Sain M, Tjong J. Emerging Trends in Automotive Lightweighting through Novel Composite Materials. Materials Sciences and Applications. 2016;7:26-38.

[27] Effects Of Hard Anodizing Aluminum Alloys On Bal Seal Performance. Bal Seal Engineering;2019.

[28] Genta; G, Morello L. The Automotive Chassis. Vol 22009.

[29] Jeyapandiarajan P, Kalaiarassan G, Joel J, Shirbhate R, Felix Telare F, Bhagat A. Design and Analysis of Chassis for an Electric Motorcycle. Materials Today: Proceedings. 2018;5(5, Part 2):13563-73.

[30] Sokoluk M, Cao C, Pan S, Li X. Nanoparticle-enabled phase control for arc welding of unweldable aluminum alloy 7075. Nature Communications. 2019;10(1):98.